Mineral magnetic properties of loess/paleosol couplets of the central loess plateau of China over the last 1.2 Myr

Chenglong Deng,[1] Rixiang Zhu,[1] Kenneth L. Verosub,[2] Michael J. Singer,[3] and Natasa J. Vidic[2,3,4]

Received 4 April 2003; revised 4 October 2003; accepted 23 October 2003; published 16 January 2004.

[1] We have conducted a multiparameter investigation of 15 loess-paleosol couplets (S0/L1 to S14/L15) from the Jiaodao section in the central loess plateau of China using environmental magnetic approaches coupled with soil science techniques. The magnetic parameters display systematic variations that seem to be closely related to paleoclimate variations and intensity of pedogenesis. High-temperature susceptibility curves of paleosols show a generally decreasing trend in reversibility from the base of the Lishi Formation to the Holocene black loam, possibly indicating a decrease in weathering intensity. This may reflect a long-term increase in aridity and/or a general long-term cooling trend of the interior of the Asian continent from 1.2 Ma to the present. Several samples display wasp-waisted hysteresis loops. These are most pronounced in moderately enhanced paleosols, less pronounced in the practically unaltered loess, and subdued in the well-developed paleosols, but wasp waistedness reappears in the most developed paleosols. This wasp-waistedness sequence suggests that the composition, concentration, and grain size of magnetic minerals all contribute to the hysteresis behavior of samples from the studied loess-paleosol sequence, but each factor has a different effect at different stages of pedogenesis. *INDEX TERMS:* 1540 Geomagnetism and Paleomagnetism: Rock and mineral magnetism; 1512 Geomagnetism and Paleomagnetism: Environmental magnetism; 1519 Geomagnetism and Paleomagnetism: Magnetic mineralogy and petrology; *KEYWORDS:* loess, paleosol, mineral magnetism, pedogenesis, loess plateau

Citation: Deng, C., R. Zhu, K. L. Verosub, M. J. Singer, and N. J. Vidic (2004), Mineral magnetic properties of loess/paleosol couplets of the central loess plateau of China over the last 1.2 Myr, *J. Geophys. Res.*, *109*, B01103, doi:10.1029/2003JB002532.

1. Introduction

[2] Eolian deposits cover an area of 440,000 km^2 on the loess plateau of north central China [*Liu*, 1985]. The classic loess-paleosol sequence of the central plateau was magnetostratigraphically determined two decades ago to span the last ~2.6 Myr [*Heller and Liu*, 1982]. However, more recent work has shown that the eolian deposits elsewhere go back to 22 Ma [*Guo et al.*, 2002]. Numerous studies over the past twenty years have documented that this sequence faithfully records the paleoclimatic history and variability of the East Asian monsoon since the Miocene [*Liu and Ding*, 1998; *An et al.*, 2001; *Guo et al.*, 2002]. In addition, the low-field magnetic susceptibility signal of these loess-paleosol sequences correlates well to the marine oxygen isotope record [*Heller and Liu*, 1986; *Kukla et al.*, 1988], which confirms the strong linkage between magnetic properties of the Chinese loess-paleosol sequences and the global climate record.

[3] In the classic Chinese loess-paleosol sequences, paleosols are always magnetically enhanced due to paleoclimate-driven pedogenesis [*Zhou et al.*, 1990; *Verosub et al.*, 1993; *Heller and Evans*, 1995; *Evans and Heller*, 2001]. However, paleoclimatic and paleoenvironmental interpretations of the magnetic signal of these sequences are not straightforward. Although some authors have fruitfully addressed the paleoclimate record of the sequence using multiple mineral-magnetic parameters [*Banerjee et al.*, 1993; *Hunt et al.*, 1995; *Fukuma and Torii*, 1998; *Florindo et al.*, 1999], systematic mineral magnetic data on the loess-paleosol sequence remain requisite. Here we contribute to a better understanding of the links between magnetic parameters and pedogenesis using a detailed multiparameter mineral-magnetic approach coupled with pedological methods. To this end, we describe the results of our integrated mineral magnetic and pedological investigation of 15 loess-paleosol couplets from the Jiaodao section (35.9°N, 109.4°E) in the central loess plateau. The results of our study suggest a long-term decrease in weathering intensity over the last 1.2 Myr and confirm that an integrated study of magnetic mineralogy of these couplets yields

[1] Paleomagnetism Laboratory, Institute of Geology and Geophysics, Chinese Academy of Sciences, Beijing, China.
[2] Department of Geology, University of California, Davis, California, USA.
[3] Department of Land, Air and Water Resources, University of California, Davis, California, USA.
[4] Agronomy Department, University of Ljubljana, Ljubljana, Slovenia.

0148-0227/04/2003JB002532$09.00

important information on Fe mineral transformations and their relation to pedogenesis and paleoclimate.

2. Geological Setting and Sampling

[4] The Jiaodao section (35.9°N, 109.4°E) lies in Shaanxi province, north China. It is approximately 50 km north of the classic Luochuan section (35.8°N, 109.4°E) [*Liu*, 1985; *Heller and Liu*, 1982] and consists, from top to bottom, of Holocene loess (L0) and black loam (S0), the Malan Formation (L1), the Lishi Formation (S1/L2 to S14/L15) and the Wucheng Formation (S15/L16 to S32/L33). The region has a semiarid continental climate with a mean annual precipitation of 600 mm and a mean annual temperature of 8.9°C. The annual precipitation is not evenly distributed throughout the year and about 60% of it usually falls in July, August and September. The seasonal temperature range is also quite high: with a mean July temperature of 23.3°C, and a mean January temperature of −6.5°C [*Xu and Wang*, 2003]. The present soil temperature regime is mesic, and the present soil moisture regime ustic [*Vidic et al.*, 2000].

[5] Our samples come from the upper 90 m of the Jiaodao section. They encompass 15 paleosol units (S0–S14) and 15 loess units (L1–L15). These 15 loess-paleosol couplets form a sedimentary sequence spanning the last 1.2 Myr [*Ding et al.*, 2002; *Pan et al.*, 2002]. Each couplet consists of a paleosol and its underlying parent loess horizon. We sampled the whole section at 20-cm intervals. For this study, we chose one sample from each paleosol and one from each loess layer. For each loess/paleosol couplet, we chose the paleosol sample with the highest value of magnetic susceptibility (representing maximum pedogenesis) and the loess sample with the lowest value (representing minimum pedogenesis).

3. Experimental Methods

[6] Magnetic susceptibility versus temperature curves (χ-T) were obtained by continuous exposure of samples through temperature cycles from room temperature to 700°C and back to room temperature using a KLY 3 Kappa bridge with a CS-3 high-temperature furnace (Agico Ltd., Brno). To minimize the possibility of oxidation, the samples were heated and cooled in an argon atmosphere. For each sample, the sample holder and thermocouple's contributions to susceptibility were subtracted.

[7] Hysteresis parameters of the loess and paleosols were measured using a MicroMag 2900 Alternating Gradient Magnetometer (AGM) (Princeton Measurements Corp., USA). A few milligrams of natural material were attached to the sample probe. The magnetic field was then cycled between ±1.5 T for each sample. Saturation magnetization (M_s), saturation remanence (M_{rs}), and coercivity (B_c) were determined after the correction for the paramagnetic contribution identified from the slope at high fields. Samples were then demagnetized in alternating fields (AF) up to 250 mT, and an isothermal remanent magnetization (IRM) was imparted from 0 to 1.5 T also using the MicroMag 2900 AGM. Subsequently the IRM at 1.5 T was demagnetized in a stepwise backfield from 0 to −1.5 T to obtain coercivity of remanence (B_{cr}). The paramagnetic susceptibility (χ_p) was calculated from the linear part of the closed hysteresis loop between 0.7 T and 1.5 T. The ferrimagnetic susceptibility (χ_f) was calculated from $\chi_f = \chi - \chi_p$. For some selected samples, anhysteretic remanent magnetization (ARM) was acquired in a 50 μT DC field superimposed on a peak AF demagnetizing field of 100 mT. The ARM was then measured and stepwise AF demagnetized up to 60 mT at 10 mT intervals using a 2G Enterprises 755-R cryogenic magnetometer.

[8] To investigate the weathering intensity of the loess and paleosol samples further, we made additional soil physics and soil chemistry measurements. Munsell color was determined using a CR-200 Chroma Meter (Minolta, Japan). In addition, all samples were treated with a citrate-bicarbonate-dithionite (CBD) procedure [*Janitzky*, 1986]. For each sample, we measured low-field magnetic susceptibility both before and after CBD treatment using a Bartington MS-2 susceptibility meter. The free iron (Fe_d) concentration was measured in the CBD extract using inductively coupled plasma spectrometry with an IRIS Plasma Spectrometer (Thermo Jarrell Ash Corp., USA).

4. Results

4.1. High-Temperature Susceptibility Measurements

[9] Temperature-dependent susceptibility is highly sensitive to mineralogical changes during thermal treatment, but such changes can provide information about magnetic mineral composition and magnetic grain size [*Dunlop and Özdemir*, 1997]. It has been shown that the Chinese loess/paleosols contain some thermally unstable components, such as iron-bearing clay minerals and maghemite, whose transformation during thermal cycling can be traced by changes in susceptibility [*Hunt et al.*, 1995; *Florindo et al.*, 1999; *van Velzen and Dekkers*, 1999; *Deng et al.*, 2001; *Zhu et al.*, 2001].

[10] Figure 1 illustrates the temperature-dependent susceptibility variations of the 15 loess-paleosol couplets of the Jiaodao section. All the χ-T curves are characterized by a major decrease in susceptibility at about 585°C, the Curie point of magnetite. This behavior indicates that magnetite is the major contributor to the susceptibility. The heating curves also reach a maximum between 150°C and 300°C. This behavior is more pronounced for paleosols than for loess. This susceptibility maximum may arise from the reduction of hematite to magnetite when heating organic matter in samples, or from the neoformation of minor ferrimagnetic phases during heating, e.g., maghemite [*Oches and Banerjee*, 1996]. It is unlikely that the production of these ferrimagnetic phases results from decomposition of lepidocrocite because these loess and paleosols are well drained. This maximum is followed by a steady decrease in susceptibility extending to at least 450–500°C. Previously reported thermomagnetic behavior (J_S-T curves) of some Chinese loess/paleosol samples also showed a decrease during heating beginning near 300°C [*Evans and Heller*, 1994; *Zhu et al.*, 1994; *Liu et al.*, 2003]. We agree with the suggestion that the decrease in susceptibility probably results from thermally induced conversion of metastable maghemite to hematite [*Oches and Banerjee*, 1996; *Florindo et al.*, 1999; *Zhu et al.*, 2001; *Guo et al.*, 2001]. Although it has been established by mineral magnetic

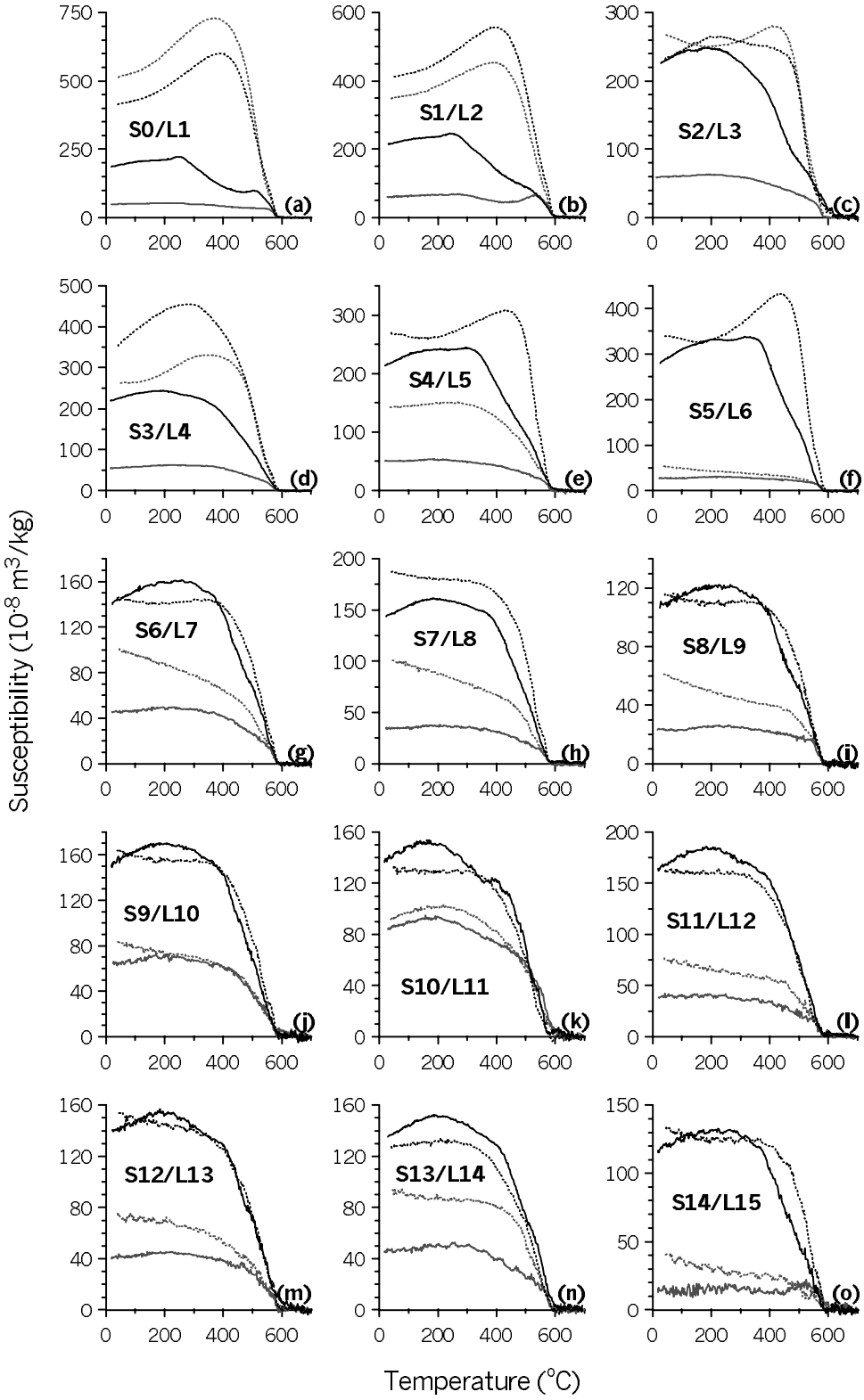

Figure 1. The χ-T curves of typical samples from the loess-paleosol sequence at Jiaodao. Thin (thick) lines represent loess (paleosol) samples. Solid (dotted) lines represent heating (cooling) curves.

analysis [*Evans and Heller*, 1994] and by X-ray spectra [*Zhu et al.*, 1994; *Deng et al.*, 2000], that hematite coexists with magnetite in the loess and paleosol samples, the contribution of this mineral to the susceptibility is not significant [*Fine et al.*, 1995; *Vidic et al.*, 2000].

[11] The heating curves of S0, L2 and L15 display a noteworthy secondary peak at about 520°C (Figures 1a, 1b, and 1o), but other loess and paleosol units do not exhibit such behavior. The fact that this feature is not seen in the cooling curves suggests that we are not dealing with a

Table 1. Rock Magnetism and Soil Science Data for the Loess and Paleosols of the Jiaodao Section

Stratigraphy	χ, 10^{-8} m^3/kg	χ_p, 10^{-8} m^3/kg	χ_f, 10^{-8} m^3/kg	M_{rs}, 10^{-3} A m^2/kg	M_s, 10^{-3} A m^2/kg	B_c, mT	B_{cr}, mT	S Ratio	Fe_d, %	Munsell Code (Moist State)
S0	188.14	7.46	180.68	18.43	117.10	9.31	24.07	0.96	1.48	4.6YR 3.8/1.5
L1	48.70	4.22	44.48	5.71	39.37	13.10	46.10	0.89	0.95	7.0YR 4.7/1.9
S1	214.03	5.21	208.82	13.73	81.66	8.47	23.08	0.92	1.41	4.9YR 4.2/1.9
L2	60.81	4.92	55.89	6.07	46.51	11.07	40.14	0.94	1.13	5.6YR 4.6/2.1
S2	226.27	7.97	218.30	12.85	76.33	8.70	22.93	0.97	1.57	3.6YR 4.4/2.0
L3	59.40	4.97	54.43	6.43	41.61	12.69	40.96	0.90	1.01	6.6YR 4.6/2.3
S3	221.06	7.52	213.54	18.10	114.60	8.28	22.26	0.96	1.54	2.4YR 4.7/1.7
L4	55.06	4.45	50.61	5.85	34.00	13.33	42.16	0.88	1.03	6.2YR 4.5/2.5
S4	215.04	7.71	207.33	15.00	90.92	9.26	22.55	0.97	1.49	2.8YR 4.8/1.6
L5	50.96	4.71	46.25	5.62	31.79	14.26	45.55	0.88	1.02	6.1YR 4.9/2.3
S5	280.09	8.06	272.03	25.34	145.69	8.92	23.45	0.87	1.82	1.9YR 4.2/1.9
L6	27.85	4.60	23.25	4.37	23.99	18.70	59.92	0.80	0.96	7.2YR 5.0/2.1
S6	141.03	6.69	134.34	11.36	64.06	10.53	27.86	0.88	1.54	3.3YR 4.6/2.0
L7	45.59	3.58	42.01	5.10	29.28	14.78	46.42	0.83	0.93	6.3YR 4.9/2.4
S7	142.05	6.50	135.55	11.23	67.08	9.69	26.23	0.87	1.35	3.4YR 4.7/1.9
L8	34.79	3.22	31.57	4.15	19.26	17.93	51.62	0.84	0.87	7.0YR 5.0/2.4
S8	105.40	5.93	99.47	11.62	62.20	9.83	25.08	0.88	1.45	4.7YR 4.5/2.3
L9	23.27	3.34	19.93	4.22	19.71	23.22	70.52	0.79	1.02	6.7YR 5.0/2.2
S9	150.81	7.33	143.48	12.29	71.00	9.82	26.93	0.87	1.43	3.7YR 4.3/2.4
L10	63.19	5.25	57.94	6.83	37.28	13.37	41.03	0.84	1.08	5.6YR 5.2/2.3
S10	137.34	6.01	131.33	9.26	53.19	9.85	27.11	0.87	1.27	4.6YR 4.7/2.6
L11	83.91	6.81	77.10	8.58	44.59	11.06	34.85	0.87	1.33	4.2YR 5.0/2.4
S11	160.99	6.82	154.17	12.57	71.27	9.24	23.37	0.87	1.34	3.6YR 4.8/2.4
L12	40.15	4.42	35.73	4.83	24.76	15.86	48.17	0.80	0.95	6.3YR 5.4/2.3
S12	139.56	5.87	133.69	11.57	65.23	9.99	27.27	0.88	1.18	3.9YR 4.7/2.6
L13	39.93	5.89	34.04	5.87	31.69	13.45	42.22	0.81	1.01	5.8YR 4.9/2.8
S13	135.28	7.23	128.05	13.99	79.73	8.55	23.41	0.86	1.38	5.1YR 4.7/2.3
L14	44.32	5.17	39.15	6.34	34.13	13.81	42.35	0.84	1.07	6.3YR 4.9/2.5
S14	114.91	4.07	110.84	6.66	34.33	11.60	33.19	0.85	1.29	4.1YR 4.5/2.7
L15	16.14	2.51	13.63	2.90	12.11	24.17	63.16	0.74	0.95	6.6YR 4.8/2.3

Notes: χ, low-field susceptibility; χ_p, paramagnetic susceptibility; χ_f, ferrimagnetic susceptibility; M_s, saturation magnetization; M_{rs}, saturation remanence; B_c, coercivity; B_{cr}, coercivity of remanence; S ratio, $-IRM_{-0.3T}/SIRM_{1.5T}$; and Fe_d, free iron.

Hopkinson peak, but rather with the neoformation at moderately high temperature of a high susceptibility phase [*Deng et al.*, 2001].

[12] The cooling cycles of all samples show an increase in susceptibility when cooled below 585°C. This behavior is more pronounced for younger units than for older ones, and more pronounced for loess than for paleosols. With the exception of loess unit L5 (Figure 1e), the cooling curves of the younger loess units from the upper Lishi Formation (i.e., those younger than S5) show a marked susceptibility peak at around 400°C. This peak is followed by a clear decrease in magnetic susceptibility (Figures 1a–1d). Correspondingly, with the exception of loess unit L11 (Figure 1k), the cooling curves of the older loess units from the lower Lishi Formation (i.e., older than S5) show a gradual increase in susceptibility from 400°C to room temperature (Figures 1f–1j and 1l–1o). For each loess-paleosol couplet younger than S4, the paleosol has a high-temperature susceptibility behavior similar to that of the loess unit (Figures 1a–1d). However, the χ-T curves of the paleosols older than S5 are more or less reversible (Figures 1g–1o).

4.2. Room Temperature Susceptibility Measurements

[13] Like many other sites on the loess plateau, the Jiaodao section has high χ values in paleosol horizons and low χ values in loess layers (Table 1). The parameter χ_p is also higher in paleosols ($(6.69 \pm 1.11) \times 10^{-8}$ m^3/kg) than in loess ($(4.54 \pm 1.09) \times 10^{-8}$ m^3/kg), which suggests that more weathering of paramagnetic Fe minerals occurred in paleosols than in loess layers. The χ_p at high fields is usually interpreted as resulting from paramagnetic minerals [*Florindo et al.*, 1999; *Forster and Heller*, 1997] although antiferromagnetic hematite and/or goethite can make a minor contribution [*Forster and Heller*, 1997].

[14] Two concentration-independent parameters were used to indicate the domain state of ferrimagnetic minerals: the ratio of saturation remanence to low-field susceptibility (M_{rs}/χ), and of ferrimagnetic susceptibility to saturation magnetization (χ_f/M_s) [*Hunt et al.*, 1995; *Florindo et al.*, 1999]. M_{rs}/χ has a mean value of $(12.74 \pm 2.73) \times 10^3$A/m for the 15 loess layers and $(8.01 \pm 1.57) \times 10^3$A/m for the 15 paleosol samples (Figure 2a). The evidently lower M_{rs}/χ values in the paleosols indicate that superparamagnetic (SP) grains contribute significantly to the susceptibility enhancement in paleosols, but that loess units carry more efficient remanence carriers. The χ_f/M_s has mean values of $(1.31 \pm 0.24) \times 10^{-5}$ m/A for the 15 loess samples and $(2.15 \pm 0.47) \times 10^{-5}$ m/A for the 15 paleosol samples (Figure 2b). The tendency of χ_f/M_s to increase with χ is further evidence that the concentration of SP magnetite/maghemite grains is greater in high-χ units. Interestingly, the highest χ_f/M_s value for our sample suite occurs in the intermediately developed paleosol S14 rather than in the more highly developed paleosol units (Figure 2b).

4.3. Hysteresis Properties

4.3.1. Hysteresis Loops

[15] Hysteresis loops provide information about the coercivity spectrum and domain state of ferrimagnetic materials [*Dunlop and Özdemir*, 1997]. All the samples display a significant paramagnetic contribution. After the removal of the paramagnetic signal, the loess and paleosol

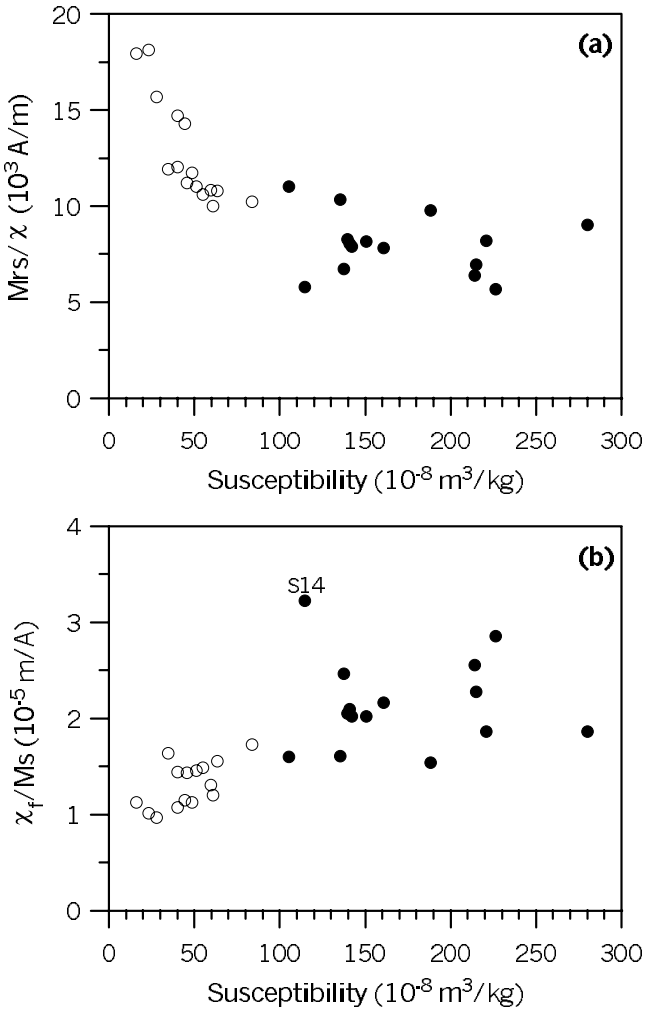

Figure 2. Variations of the ratios (a) of saturation remanence to low-field susceptibility (M_{rs}/χ) and (b) of ferrimagnetic susceptibility to saturation magnetization (χ_f/M_s) with low-field susceptibility (χ). Note that the intermediately developed soil S14 shows the highest χ_f/M_s value. Open (solid) circles represent loess (paleosol) samples.

samples exhibit different hysteresis behavior as shown in Figure 3. Most of the hysteresis loops are closed above about 350 mT for both loess and paleosol samples, which is consistent with the presence of a dominant ferrimagnetic phase. For each loess-paleosol couplet, the loop of the loess sample always closes at a higher field than that of the paleosol sample. This suggests that either the most effective remanence carriers in the loess are single-domain (SD) and/or pseudosingle-domain (PSD) magnetite grains, which have higher coercivities than SP ($B_c = 0$) and multidomain (MD) magnetite grains; or that loess contains a significantly higher amount of antiferromagnetic minerals. The loops for some low-χ units, such as L6, L9 and L15 (Figure 4) do not close even at 500 mT. We interpret this behavior as arising from higher ratios of hematite to magnetite in these practically unaltered loess units compared to more weathered loess units, although low-temperature oxidation of magnetite to maghemite could also partly contribute to the higher coercivities [*van Velzen and Dekkers*, 1999; *Liu et al.*, 2003]. Moreover, loess samples with low χ have wide hysteresis loops, especially the two sandy loess layers L9 and L15, while paleosol samples with high χ display narrow hysteresis loops, especially the well-developed paleosol horizons S3, S4 and S5.

[16] Some loess and paleosol samples display wasp-waisted hysteresis loops (Figure 4). The degree of wasp waistedness varies systematically with χ. As reported by *Fukuma and Torii* [1998] for the Luochuan section, samples with the lowest χ, such as L6, L9 and L15 (Figures 4b, 4d, and 4f) in our sample suite, have loops that are slightly wasp waisted, while samples with intermediate χ, such as S14 (Figure 4e), show pronounced wasp-waisted behavior. The wasp-waisted character becomes almost indiscernible in moderately well-developed paleosols, such as S3 (Figure 4a), but it becomes evident again as χ increases further. For example, the most developed paleosol S5 (Figure 4c) has a more wasp-waisted curve than S3. The reappearance of wasp waistedness in the most developed paleosols was not observed by *Fukuma and Torii* [1998].

4.3.2. Hysteresis Parameters

[17] Values of M_{rs}/M_s versus B_{cr}/B_c for our loess and paleosol samples are plotted in Figure 5 on a Day diagram [*Day et al.*, 1977; *Dunlop*, 2002]. Since the primary magnetic carrier is magnetite/maghemite, this diagram can be used to deduce that the average magnetic grain size falls in PSD range for both loess and paleosols. Also, in the Day plot, the paleosol samples are more tightly clustered than the loess samples. It should be pointed out that the presence of SP grains could offset the M_{rs} of stably magnetized SD or larger grains, which would produce anomalously low values of B_c [*Dunlop and Özdemir*, 1997], and that the presence of high-coercivity components (hematite and/or goethite) could lead to increasing B_{cr}, and hence increasing the values of B_{cr}/B_c [*Roberts et al.*, 1995]. As a consequence, the hysteresis parameters will shift to the coarser end of the PSD window to some extent.

[18] M_{rs}/M_s is fairly uniform throughout the investigated section, with a mean value of 0.18 ± 0.03 for the 15 loess samples and 0.17 ± 0.01 for the 15 paleosol samples. This behavior suggests that not only SP but also SD and/or PSD magnetite grains form during pedogenesis. Otherwise, there should be a larger difference between mean values of loess and paleosols.

[19] M_s and M_{rs} increase linearly with χ both in loess and in paleosols (Figures 6a and 6b). M_s and M_{rs} of the loess samples correlate well with χ, with correlation coefficients of R = 0.90 and R = 0.94, respectively. M_s and M_{rs} of the paleosol samples correlate with χ as well, but with lower correlation coefficients of R = 0.83 and R = 0.81, respectively. This linear behavior indicates that the increase in ferrimagnetic mineral concentration makes a significant contribution to the enhanced susceptibility, as suggested by *Eyre and Shaw* [1994], *Forster and Heller* [1997] and *Florindo et al.* [1999]. However, we note that for the significantly enhanced paleosols, the increase of M_s and M_{rs} with increasing χ tends to be less linear than for the weakly enhanced loess material.

[20] Loess and paleosols do not show significant differences in their remanence ratios (M_{rs}/M_s), but loess samples

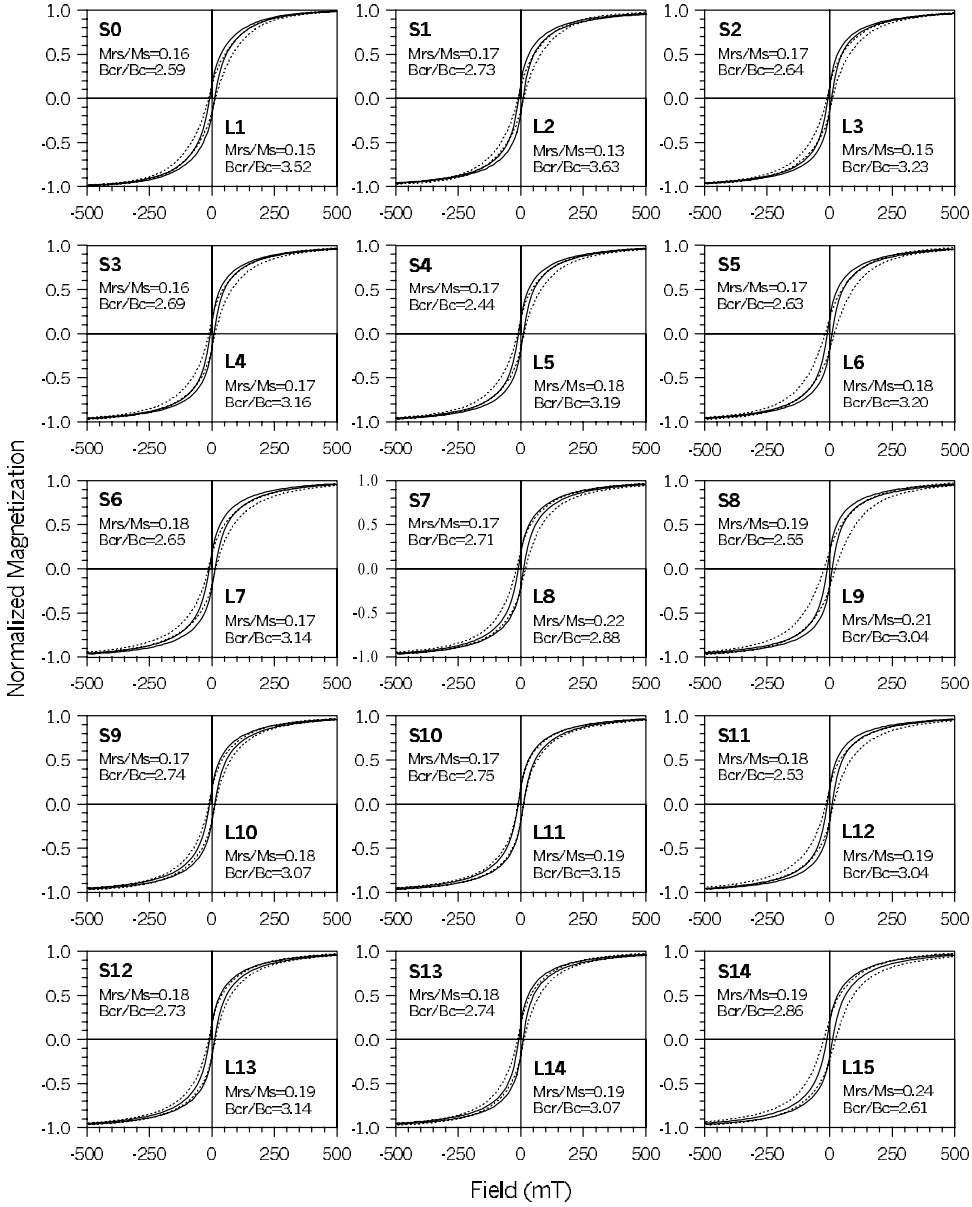

Figure 3. Comparison of hysteresis loops (corrected for paramagnetism) for the loess-paleosol couplets of the Jiaodao section. Loops drawn with the dotted and solid lines represent loess and paleosol units, respectively.

exhibit rather higher coercivity ratios (B_{cr}/B_c). Paleosols have systematically lower B_c and B_{cr} values compared to the loess. B_c has mean values of 15.39 ± 3.98 mT for loess and 9.47 ± 0.87 mT for paleosols. B_{cr} has mean values of 47.68 ± 9.77 mT for loess and 25.25 ± 2.92 mT for paleosols. The maximum values of B_c and B_{cr} occur in the loess units. The differences in B_c between loess and paleosols are partly or mostly due to the larger proportion of SP material in the paleosols, which can result in a lower value of B_c, but has no effects on B_{cr} [*Liu et al.*, 2003]. However, the differences in B_{cr} are probably driven by higher antiferromagnetic proportions and perhaps also relatively higher SD/PSD ferrimagnetic proportions in the loess units [*Day et al.*, 1977; *Roberts et al.*, 1995; *Fukuma and Torii*, 1998]. For our sample suite, both B_c and B_{cr} decrease with increasing χ, but trend asymptotically toward minimum values of 7.6 mT and 21.5 mT, respectively (Figure 6c). In addition, there exists a strong linear dependence between B_c and B_{cr} (Figure 6d).

4.4. IRM Acquisition and ARM Demagnetization

[21] The IRM acquisition curves from loess and paleosol samples display different behavior (Figure 7a). For paleosol samples, the rapid rise below 100 mT indicates the presence of magnetically soft components, such as magnetite and maghemite. The curves of loess samples suggest relatively higher coercivity phases. We note that paleosol S14 has the lowest $IRM_{0.3T}/IRM_{1.5T}$ value among the six samples shown in Figure 7a. This behavior suggests that the IRM contributed by antiferromagnetic minerals (hematite and possibly goethite) at high fields is not negligible in the paleosols. However, our magnetic measurements fail to

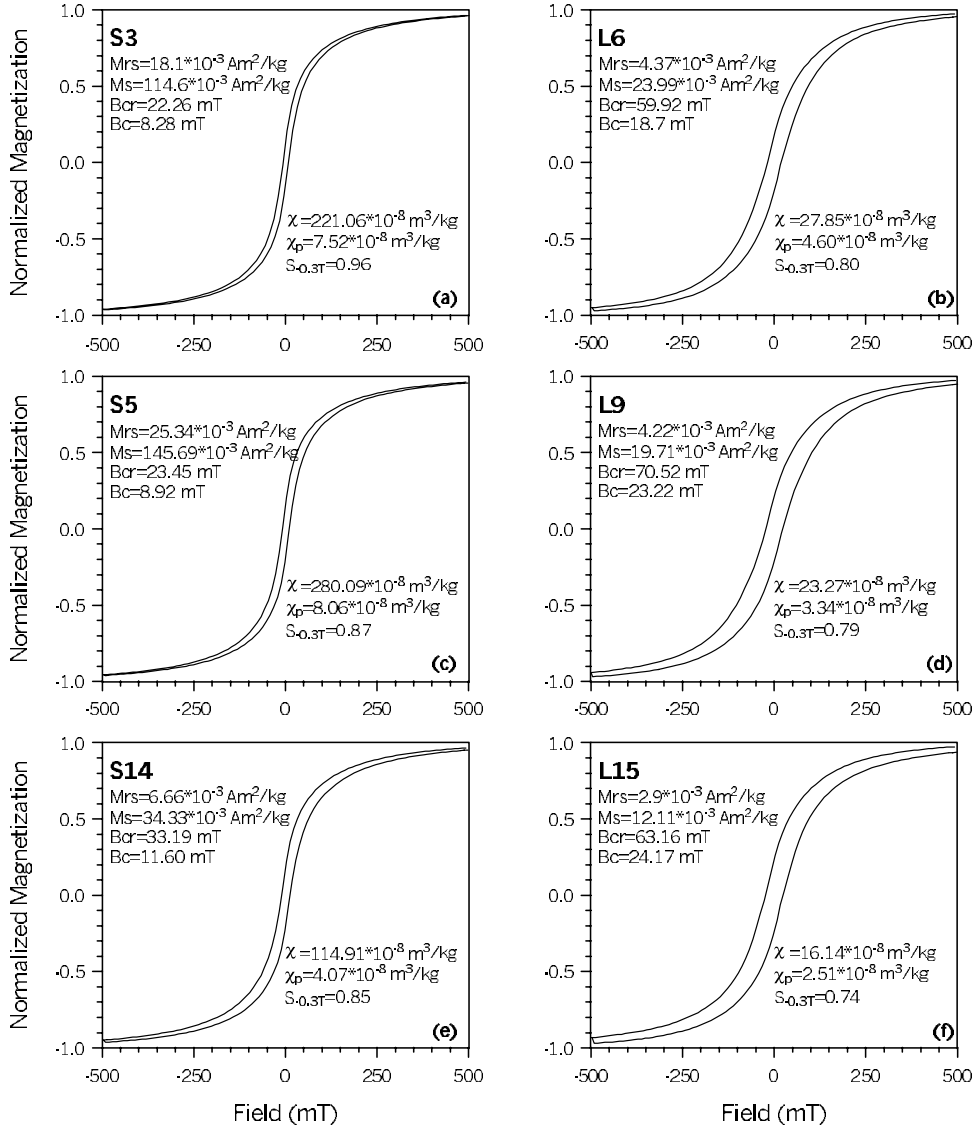

Figure 4. Examples of wasp-waisted hysteresis loops. Paramagnetic contributions were subtracted.

confirm whether or not goethite is present. The median remanent acquisition field (MAF), the field at which one-half of the saturation IRM is achieved in the forward direction, can be used for further quantitative characterization of the IRM curves, as was done by *Evans and Rokosh* [2000] and *Zhu et al.* [2003]. The MAF of the paleosols shows a fairly narrow range between 38 mT and 54 mT with a mean value of 45 ± 4 mT. This indicates similar coercivity spectra in the paleosols, even though the saturation IRMs differ significantly. The MAF of the less weathered loess samples shows a wider range from 47 mT to 73 mT with a mean value of 60 ± 8 mT. The more scattered values are probably related to the more varied degree of pedogenesis in the loess horizons. Both MAF and B_{cr} data indicate that the paleosols are magnetically softer than the loess due to stronger weathering.

[22] ARM is mainly carried by the SD and PSD particles. The higher ARM intensity of the paleosols suggests that SD and PSD particles are enriched due to pedogenesis [*Zhou et al.*, 1990; *Hunt et al.*, 1995; *Maher and Thompson*, 1991]. ARM demagnetization curves reflect the magnetic hardness of a material. Loess and paleosols have different behavior during AF demagnetization of the ARM (Figure 7b). The loess has a higher median destructive field (MDF), and its ARM demagnetization shows a broad distribution of MDFs. By contrast, paleosols have lower MDFs, and ARM demagnetization shows a more restricted distribution of MDFs. These behaviors, which are consistent with those reported by *Evans and Heller* [1994], further suggest that there are relatively higher portions of magnetically harder SD and PSD magnetite/maghemite grains in loess than in paleosols, although the absolute quantity of SD and PSD particles in the well-developed paleosols is much greater than in the less weathered loess.

4.5. *S* Ratio

[23] *S* ratio was used to assess magnetic mineralogy in loess and paleosols (Figure 8), where *S* is the absolute value of the IRM remaining after exposure to a reversed field of 0.3 T divided by the saturation IRM (or SIRM), which is usually acquired in a field of 1–2 T [*King and Channell*, 1991].

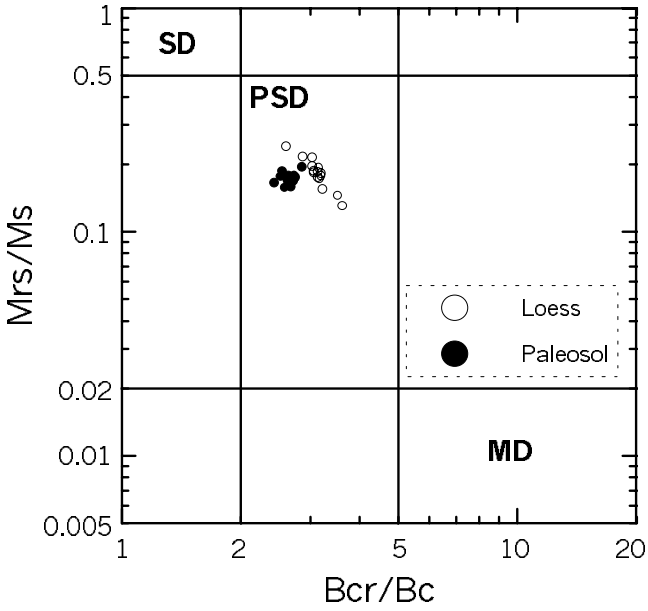

Figure 5. Hysteresis ratios plotted on a Day diagram [*Day et al.*, 1977; *Dunlop*, 2002] of the loess (open symbols) and paleosol (solid symbols) samples of the Jiaodao section. SD, single domain; PSD, pseudosingle-domain; and MD, multidomain.

$$S = (-\mathrm{IRM}_{-0.3\mathrm{T}})/(\mathrm{SIRM}_{1.5\mathrm{T}}).$$

This parameter serves as a measure of the proportion of higher coercivity minerals (i.e., hematite and goethite) to lower coercivity minerals (i.e., magnetite and maghemite) in a material [*King and Channell*, 1991; *Roberts et al.*, 1995; *Verosub and Roberts*, 1995]. For most samples, the *S* values are close to 1.0, suggesting low-coercivity and ferrimagnetic mineralogy. In particular, the significantly enhanced paleosol units, such as S2, S3 and S4, show the highest *S* values. Moreover, weakly enhanced loess units, such as the two sandy loess horizons L9 and L15, are characterized by the lowest *S* values, which implies a significant contribution from high-coercivity antiferromagnetic minerals (mainly hematite) and/or from SD/PSD magnetite grains. In addition, the most enhanced paleosol S5 shows an obviously lower *S* value than other well-developed paleosol units (e.g., S2, S3 and S4), indicating a higher portion of antiferromagnetic minerals.

4.6. Soil Reddening

[24] Munsell colors (Table 1) were measured to evaluate the intensity of soil reddening (rubification). Almost all loess units exhibit a yellow color and very weak rubification, possibly signaling the presence of goethite [*Ji et al.*, 2001]. In particular, the last glacial loess L1 and the two sandy loess units L9 and L15 have an obviously paler color

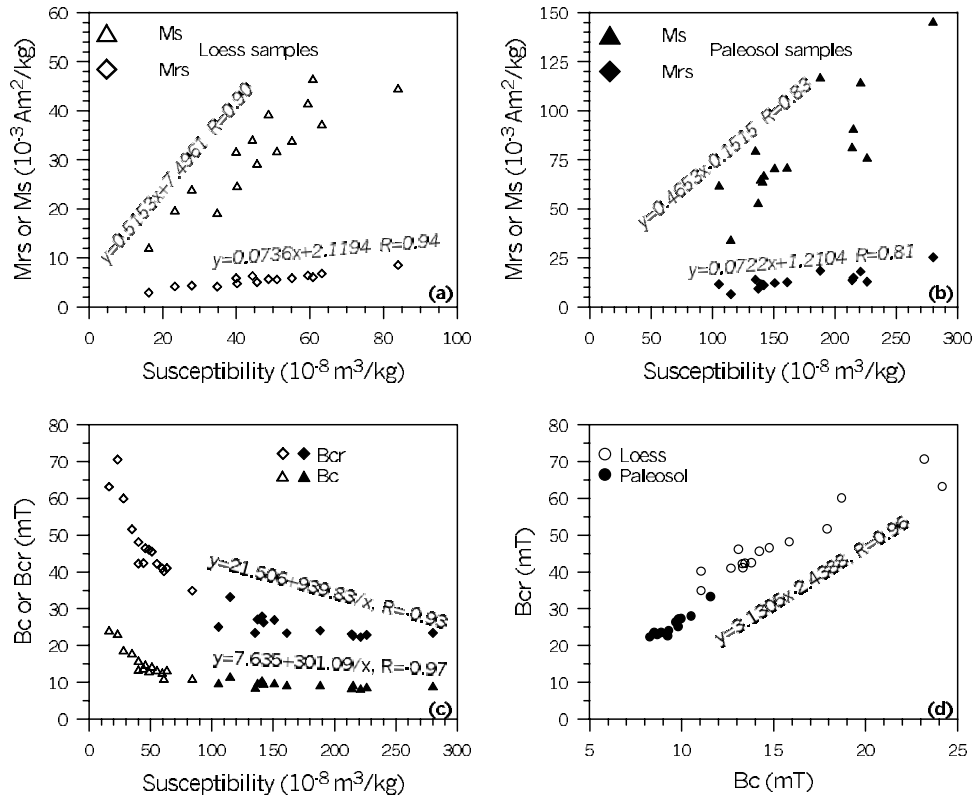

Figure 6. (a) Saturation magnetization (M_s) and saturation remanence (M_{rs}) versus low-field susceptibility (χ) for loess units. (b) M_s and M_{rs} versus χ for paleosol units. (c) Coercivity (B_c) and coercivity of remanence (B_{cr}) versus χ for the studied loess and paleosols. (d) A good linear relationship between B_c and B_{cr}.

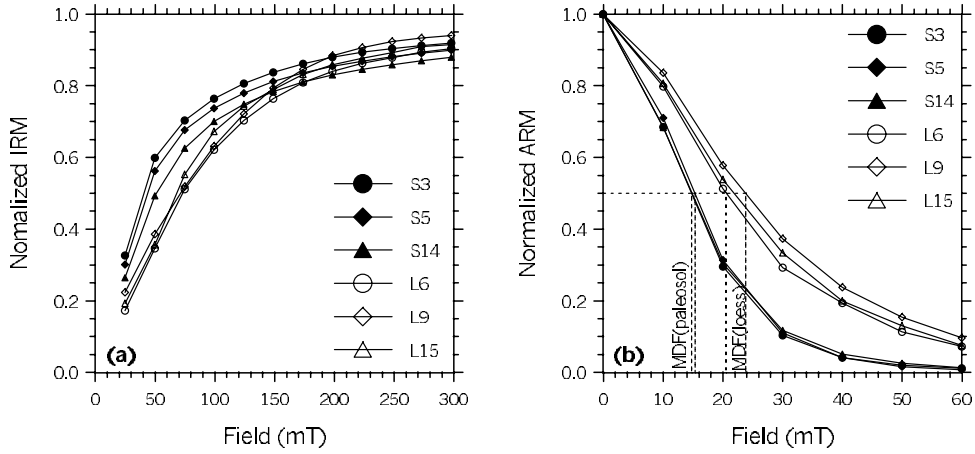

Figure 7. (a) IRM acquisition and (b) ARM demagnetization curves of the selected loess and paleosol samples. The IRM curves, which are obtained in the applied field up to 1500 mT, are cut off at 300 mT for reasons of clarity. Note that loess units have higher MDF of ARM than paleosols.

than other loess units. This characteristic, together with the massive structure and high $CaCO_3$ concentrations [*Liu*, 1985], suggests that negligible chemical weathering occurred after loess accumulation in glacial intervals. The Holocene soil S0 and the last interglacial soil S1 have a dark color and fairly weak rubification. The older paleosol horizons are significantly rubified, possibly indicative of high contents of hematite [*Ji et al.*, 2001]. With hues of 2–2.5 YR in a moist state, S3, S4 and S5 represent the most rubified paleosols. These paleosols are characterized by abundant reddish iron oxide/hydroxides particles in the fine fraction. The prominent rubification of the most developed paleosol S5 with high χ is widely used as a stratigraphic marker horizon in field investigations [*Liu*, 1985; *Guo et al.*, 1998; *Ding et al.*, 2002].

[25] On the loess plateau, the well-drained, fine-textured eolian deposits, which have low organic content and nearly neutral pH [*Maher*, 1998], favor efficient rubification during warm and humid interstadial and interglacial periods. For example, the most developed paleosols S4 and S5, which were formed under subtropical semihumid climates [*Guo et al.*, 1998], display the most intense rubification in the studied loess-paleosol sequence. Although detrital hematite is possibly present in the most rubified paleosols, we argue that the reddening of paleosols developed on fine-grained loess in the central loess plateau indicates the predominance of climatically controlled pedogenic processes rather than lithogenic effects. Associated with other processes, rubification of paleosols in Chinese eolian deposits can be considered as an indication of warmer and moister environments than present-day conditions.

4.7. Soil Chemistry

[26] After CBD extraction, low-field magnetic susceptibilities of loess layers decrease by 26% to 85%, with a mean post-CBD χ value of $(13.32 \pm 2.94) \times 10^{-8}$ m^3/kg. For paleosol samples, susceptibilities decrease by 89% to 96%, and have a mean post-CBD χ value of $(13.52 \pm 2.34) \times 10^{-8}$ m^3/kg. The post-CBD susceptibilities are statistically identical for the loess and paleosols, and significantly lower than almost all of the untreated loess. The low value and narrow range of susceptibilities for the CBD-extracted samples demonstrate that lithogenic magnetite grains with low and nearly uniform concentrations [*Verosub et al.*, 1993; *Fine et al.*, 1995; *Deng et al.*, 2000; *Vidic et al.*, 2000], which are mainly large PSD and MD-like magnetite grains (C. Deng et al., manuscript in preparation, 2003), are present in the Jiaodao loess/paleosol couplets over the last 1.2 Myr. The features would imply that even the loess units have been pedogenically enhanced to varying degrees,

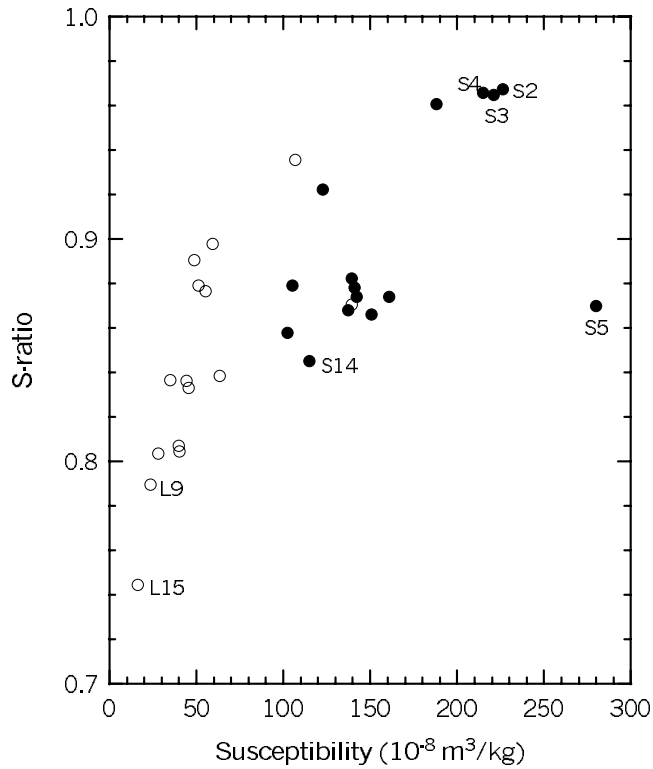

Figure 8. *S* ratio versus susceptibility for loess (open circles) and paleosol (solid circles) samples.

which is consistent with the presence of a significant SP fraction suggested by the fairly high mean ratio of χ_f/M_s in both paleosols and loess units (Figure 2b). Values of Fe_d are higher in the strongly weathered paleosols (1.44% ± 0.15%) than in the weakly weathered loess (1.02% ± 0.11%) (Table 1). The higher values of CBD-extractable susceptibility and Fe_d in the paleosols reflect the effects of stronger pedogenesis [*Verosub et al.*, 1993; *Vidic et al.*, 2000; *Ding et al.*, 2001]. Following the approach of *Vidic et al.* [2000], we plotted free iron concentration against the CBD-extracted susceptibility (Figure 9). A linear relationship was observed, corresponding to an increase in CBD-extracted susceptibility of about 274×10^{-8} m^3/kg for each 1% increase in Fe_d. According to the calculation of *Vidic et al.* [2000], if the 1% of Fe_d is present in the form of pure magnetite and maghemite, its contribution to the susceptibility would be about $(860 \sim 1390) \times 10^{-8}$ m^3/kg. This suggests that only 20% ∼ 32% of the 1% increase in Fe_d corresponds to pedogenic magnetite and maghemite. Our results confirm those of *Vidic et al.* [2000], who estimate that most of the Fe_d in paleosols is in the form of antiferromagnetic minerals, such as hematite and possibly goethite, which contribute little to the magnetic susceptibility. In this sense, antiferromagnetic components dominate the magnetic mineralogy in Chinese loess and paleosols, as previously inferred from magnetic measurements [*Evans and Heller*, 1994].

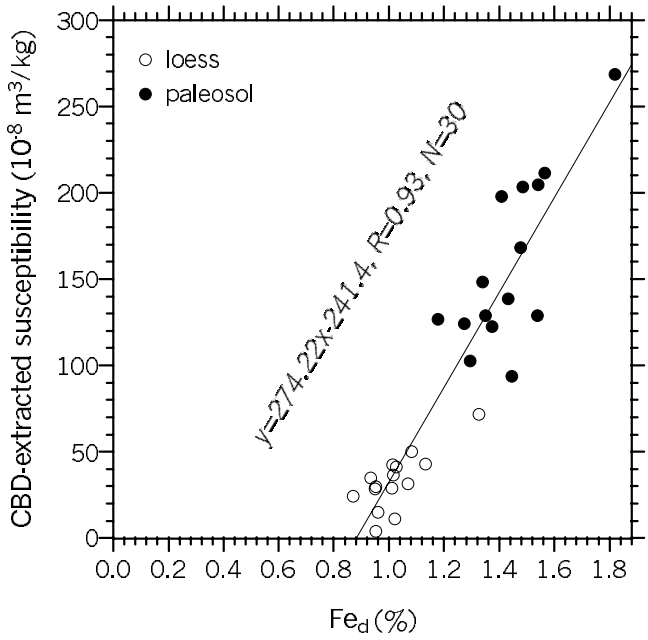

Figure 9. CBD-extracted susceptibility versus free iron (Fe_d) concentration for loess and paleosols of the Jiaodao section.

5. Discussion

5.1. Paleoclimatic Interpretation of the High-Temperature Susceptibility Measurements

[27] The high-temperature susceptibility data reported in this paper show several interesting patterns that provide further evidence for magnetite and maghemite as the dominant ferrimagnetic minerals in Chinese eolian deposits. For each loess-paleosol couplet, the paleosol has a significantly higher initial susceptibility. The χ-T curves for loess samples are generally less reversible than those of paleosols, and curves for younger units are less reversible than those of older ones. Postheating susceptibility values for younger samples show a greater percentage increase over preheating values than do older samples. Thus significantly more new magnetic material is produced by heating younger units. This implies that in the unweathered loess, iron must be present in some form that can be converted to a ferrimagnetic phase upon heating, and that the abundance of this form of iron is greater in the younger sediments.

[28] A significant increase in susceptibility after thermal treatment is usually attributed to the transformation of iron-containing silicates/clays [*Hunt et al.*, 1995; *Deng et al.*, 2000; *Zhu et al.*, 2001]. In Chinese loess and paleosols, chlorite and biotite are particularly ubiquitous iron-containing clay minerals [*Liu*, 1985; *Kalm et al.*, 1996; *Chen et al.*, 2000]. In natural soil environments, Fe-bearing micas such as biotite and chlorite are weatherable and prone to decomposition [*Righi et al.*, 1995]. Thus they can serve as one of the sources of iron for the production of new fine-grained magnetite/maghemite grains during pedogenesis. It has also been reported that chlorite is less abundant in the strongly weathered paleosol horizons than in the weakly weathered loess layers [*Kalm et al.*, 1996; *Chen et al.*, 2000]. We suggest that the weathering has depleted the supply of weatherable Fe minerals in paleosols and reduced the supply of iron-bearing precursor phases, leading to a relative and absolute deficiency of iron that can serve as the source for the formation of new magnetite during laboratory heating.

[29] We also observe that upon heating some new magnetite grains are formed in paleosols from the middle Lishi Formation, such as S4, S5 and S7, whereas χ-T curves of the paleosols from the lower Lishi Formation, such as S8, S9, S10, S11, S12, S13 and S14, are almost reversible (Figure 1). This decreasing trend in reversibility from the base of the Lishi Formation to the Holocene black loam possibly suggests a long-term decrease of weathering intensity from 1.2 Ma to the present, which, in turn, might be ascribed to an increase in aridity and/or to a cooling trend of the Asian continent during this period. This is further supported by a general trend since 1.2 Ma toward coarsening median grain size in the Luochuan (35.8°N, 109.4°E) loess/paleosol sequence [*Sun and Liu*, 2000], toward an increase in illite in the Baoji loess/paleosol sequence [*Kalm et al.*, 1996], and toward a decrease in the ratio of free iron to total iron (Fe_d/Fe_t) in the Xifeng (35.7°N, 107.6°E), Changwu (35.2°N, 107.7°E) [*Guo et al.*, 2000] and Lingtai (35.0°N, 107.5°E) [*Ding et al.*, 2001] loess/paleosol sequences. Although continued diagenesis [*Singer et al.*, 1992] may partly contribute the pattern deduced from the reversibility of χ-T curves, the present study and previous investigations [*Kalm et al.*, 1996; *Guo et al.*, 2000; *Sun and Liu*, 2000; *Ding et al.*, 2001] suggest that paleoclimatic change makes dominant contributions to the long-term trend of increasing aridity and/or the long-term cooling trend. As a result, we suggest that high-temperature susceptibility could serve as a useful proxy of pedogenesis and paleoclimatic change. Therefore our results provide strong sup-

port for the concept that the magnetic mineral properties of loess and paleosols depend on paleoclimate.

5.2. Pedogenic Interpretation of the Wasp-Waisted Characteristics

[30] Wasp-waisted hysteresis loops usually result from mixtures of magnetic components with different mineralogy and/or magnetic grain size [*Roberts et al.*, 1995]. Thus the interpretation of hysteresis data is not straightforward because both magnetic mineralogy and grain size can affect hysteresis properties.

[31] For our sample suite, the wasp waistedness is most pronounced in the moderately enhanced paleosols, e.g., S14 (Figure 4e), less pronounced in the practically unaltered loess, e.g., L6, L9 and L15 (Figures 4b, 4d, and 4f), and very muted in high-χ samples, e.g., S3 (Figure 4a). These observations are consistent with the results of *Fukuma and Torii*'s [1998]. Additionally, the wasp waistedness reappears in the most enhanced paleosols, e.g., S5 (Figure 4c).

[32] The variable degree of wasp waistedness has interesting pedogenic significance. As suggested by the lowest S values, the nearly unaltered loess units with the lowest χ contain the highest relative amounts of antiferromagnetic minerals. Thus the wasp-waisted loops of the lowest-χ units result primarily from the presence of an admixture of lithogenic ferrimagnetic and antiferromagnetic minerals, as suggested by *Fukuma and Torii* [1998]. The high-coercivity component in the lowest-χ loess is most likely dominated by lithogenic hematite because the eolian dusts have been subject to moderate chemical weathering in the source regions [*Gu et al.*, 1997]. Also, the low degree of rubification of loess layers (Table 1) suggests that very little hematite occurs in fine-grained pedogenic forms. The intermediate-χ units usually contain higher amounts of pedogenic SP fraction, especially the S14 paleosol from our sample suite. As deduced from relatively high χ_f/M_s and low S values (Figures 2 and 8 and Table 1), the wasp-waisted behavior of the S14 paleosol and other intermediately developed soils may result from an admixture of pedogenic ferrimagnetic SP fraction and pedogenic antiferromagnetic fraction (hematite and possibly goethite). However, with increasing pedogenic enhancement, the hysteresis loops of well (but not the most) weathered paleosols (e.g., S3) lose their wasp waistedness (Figure 4a). As pedogenic magnetic enhancement increases, the magnetic properties become controlled by the newly formed pedogenic ferrimagnetic fraction, so that the contributions from high-coercivity lithogenic hematite to the magnetic behavior of intermediately to well developed paleosols are effectively suppressed. However, with further pedogenic enhancement, the concentration of pedogenic hematite increases enough to again make a significant contribution to the remanence. Therefore the wasp-waisted behavior occurs again in the most weathered and rubified paleosol horizons, such as S5 (Figure 4c), in which the presence of a higher amount of hard-coercivity fraction is supported by the high degree of red color (1.9YR 4.2/1.9, moist) and relatively low S value (0.87).

5.3. Magnetic Susceptibility Enhancement: Composition, Grain Size, or Concentration Control?

[33] Our mineral magnetic measurements further support the general consensus that magnetite and/or maghemite produced by pedogenesis are responsible for the enhanced magnetic susceptibility in Chinese loess and paleosols. However, the pedogenic iron (Fe_d) appears to be present mainly in the form of antiferromagnetic minerals, such as hematite and goethite, whose contributions to pedogenic susceptibility are almost negligible. There is no doubt that hematite is present in loess/paleosol sequences, especially in the rubified paleosols, but the identification of goethite is still ambiguous. We note that the presence of goethite has been suggested by heavy mineral analysis [*Liu*, 1985], Mössbauer spectroscopy [*Eyre and Dickson*, 1995; *Vandenberghe et al.*, 1998] and thermal demagnetization of composite IRMs [*Fukuma and Torii*, 1998], and has been inferred from CBD treatment in conjunction with magnetic measurements [*Vidic et al.*, 2000] and diffuse reflectance spectrophotometry [*Ji et al.*, 2001]. However, we fail to positively identify the presence of goethite in our samples using rock magnetic techniques.

[34] The higher χ_f/M_s values in our paleosol samples compared to loess samples (Figure 2b and Table 1) suggest that SP grains make significant contributions to the enhanced susceptibility in paleosols. This result supports the original suggestion of *Zhou et al.* [1990] that the SP fraction produced by pedogenesis is at least partly responsible for the enhanced susceptibility in loess and paleosols. For our sample suite, the increase in M_{rs} and ARM in paleosols indicates that coarser grains spanning the SD/PSD range are also produced during pedogenesis. Both M_{rs} and M_s increase with increasing χ, indicating that the increase in concentration also makes significant contributions to magnetic enhancement. Therefore our results show that variations not only in grain size but also in concentration lead to magnetic enhancement. This is in good agreement with the results of the Xining section (36.6°N, 101.7°E), from the western part of the loess plateau [*Hunt et al.*, 1995].

6. Conclusions

[35] 1. This study shows that a combination of several mineral magnetic measurements with soil science techniques represents a powerful multiproxy approach for the investigation of loess-paleosol sequences. In particular, high-temperature and high-field magnetic properties exhibit systematic variations that can be directly related to magnetic mineral transformations by pedogenic processes.

[36] 2. A general decrease in the reversibility of the paleosol χ-T curves from the base of the Lishi Formation to the Holocene black loam possibly suggests a long-term decrease in weathering intensity from 1.2 Ma to the present which may be ascribed to a long-term increase in aridity and/or cooling trend of the interior of the Asian continent. Consequently, the variability of high-temperature susceptibility could serve as a useful measure of pedogenesis and paleoclimatic change.

[37] 3. Although the magnetic behavior of the studied loess-paleosol sequence is dominated by ferrimagnetic assemblage of admixtures of PSD and SP grains, in some cases antiferromagnetic minerals (hematite and possibly goethite) also contribute significantly to the magnetic properties. Thus our results confirm that the mineral magnetic properties result from mixed assemblages of multiple mag-

netic components with different mineralogy, concentration and grain size.

[38] 4. The magnetic variations in Chinese loess and paleosols are jointly controlled by the changes in composition, concentration and grain size, but each variable has different effects at different stages of pedogenesis.

[39] **Acknowledgments.** High-temperature susceptibility and hysteresis measurements were carried out in the Paleomagnetism Laboratory of the Institute of Geology and Geophysics, Beijing. ARM and soil science measurements were made in the University of California, Davis. We thank the anonymous Associate Editor, M. J. Jackson, and an anonymous reviewer for their insightful comments and suggestions for improvement of the manuscript. This research was supported by NSFC grants 40104001 and 40221402, U.S. NSF grant EAR-97 10051, and R Slovenia MZT grant J4-1423-486-9.

References

An, Z., J. E. Kutzbach, W. L. Prell, and S. C. Porter (2001), Evolution of Asian monsoons and phased uplift of the Himalaya-Tibetan plateau since late Miocene times, *Nature*, *411*, 62–66.

Banerjee, S. K., C. P. Hunt, and X. M. Liu (1993), Separation of local signals from the regional paleomonsoon record of the Chinese loess plateau: A rock-magnetic approach, *Geophys. Res. Lett.*, *20*, 843–846.

Chen, J., J. Ji, Y. Chen, Z. An, J. A. Dearing, and Y. Wang (2000), Use of rubidium to date loess and paleosols of the Luochuan sequence, central China, *Quat. Res.*, *54*, 198–205.

Day, R., M. Fuller, and V. A. Schmidt (1977), Hysteresis properties of titanomagnetites: Grain-size and compositional dependence, *Phys. Earth Planet. Inter.*, *13*, 260–267.

Deng, C., R. Zhu, K. L. Verosub, M. J. Singer, and B. Yuan (2000), Paleoclimatic significance of the temperature-dependent susceptibility of Holocene loess along a NW-SE transect in the Chinese loess plateau, *Geophys. Res. Lett.*, *27*, 3715–3718.

Deng, C., R. Zhu, M. J. Jackson, K. L. Verosub, and M. J. Singer (2001), Variability of the temperature-dependent susceptibility of the Holocene eolian deposits in the Chinese loess plateau: A pedogenesis indicator, *Phys. Chem. Earth, Part A*, *26*, 873–878.

Ding, Z. L., S. L. Yang, J. M. Sun, and T. S. Liu (2001), Iron geochemistry of loess and red clay deposits in the Chinese Loess Plateau and implications for long-term Asian monsoon evolution in the last 7.0 Ma, *Earth Planet. Sci. Lett.*, *185*, 99–109.

Ding, Z. L., E. Derbyshire, S. L. Yang, Z. W. Yu, S. F. Xiong, and T. S. Liu (2002), Stacked 2.6-Ma grain size record from the Chinese loess based on five sections and correlation with the deep-sea $\delta^{18}O$ record, *Paleoceanography*, *17*(3), 1033, doi:10.1029/2001PA000725.

Dunlop, D. J. (2002), Theory and application of the Day plot (M_{rs}/M_s versus H_{cr}/H_c): 1. Theoretical curves and tests using titanomagnetite data, *J. Geophys. Res.*, *107*(B3), 2076, doi:10.1029/2001JB000486.

Dunlop, D. J., and Ö. Özdemir (1997), *Rock Magnetism: Fundamentals and Frontiers*, 573 pp., Cambridge Univ. Press, New York.

Evans, M. E., and F. Heller (1994), Magnetic enhancement and palaeoclimate: A study of a loess/palaeosol couplet across the Loess Plateau of China, *Geophys. J. Int.*, *117*, 257–264.

Evans, M. E., and F. Heller (2001), Magnetism of loess/paleosol sequences: Recent developments, *Earth Sci. Rev.*, *54*, 129–144.

Evans, M. E., and C. D. Rokosh (2000), The last interglacial in the Chinese Loess Plateau: A petromagnetic investigation of samples from a north-south transect, *Quat. Int.*, *68–71*, 77–82.

Eyre, J. K., and D. P. E. Dickson (1995), Mössbauer spectroscopy analysis of iron-containing minerals in the Chinese loess, *J. Geophys. Res.*, *100*, 17,925–17,930.

Eyre, J. K., and J. Shaw (1994), Magnetic enhancement of Chinese loess-The role of γFe_2O_3?, *Geophys. J. Int.*, *117*, 265–271.

Fine, P., K. L. Verosub, and M. J. Singer (1995), Pedogenic and lithogenic contributions to the magnetic susceptibility record of the Chinese loess/paleosol sequence, *Geophys. J. Int.*, *122*, 97–107.

Florindo, F., R. Zhu, B. Guo, L. Yue, Y. Pan, and F. Speranza (1999), Magnetic proxy climate results from the Duanjiapo loess section, southernmost extremity of the Chinese loess plateau, *J. Geophys. Res.*, *104*, 645–659.

Forster, T., and F. Heller (1997), Magnetic enhancement paths in loess sediments from Tajikistan, China and Hungary, *Geophys. Res. Lett.*, *24*, 17–20.

Fukuma, K., and M. Torii (1998), Variable shape of magnetic hysteresis loops in the Chinese loess-paleosol sequence, *Earth Planets Space*, *50*, 9–14.

Gu, Z. Y., D. Lal, T. S. Liu, Z. T. Guo, J. Southon, and M. W. Caffee (1997), Weathering histories of Chinese loess deposits based on uranium and thorium series nuclides and cosmogenic ^{10}Be, *Geochim. Cosmochim. Acta*, *61*, 5221–5231.

Guo, B., R. X. Zhu, A. P. Roberts, and F. Florindo (2001), Lack of correlation between paleoprecipitation and magnetic susceptibility of Chinese loess/paleosol sequences, *Geophys. Res. Lett.*, *28*, 4259–4562.

Guo, Z., T. Liu, N. Fedoroff, L. Wei, Z. Ding, N. Wu, H. Lu, W. Jiang, and Z. An (1998), Climate extremes in loess of China coupled with the strength of deep-water formation in the North Atlantic, *Global Planet. Change*, *18*, 113–128.

Guo, Z., P. Biscaye, L. Wei, X. Chen, S. Peng, and T. Liu (2000), Summer monsoon variations over the last 1.2 Ma from the weathering of loess-soil sequences in China, *Geophys. Res. Lett.*, *27*, 1751–1754.

Guo, Z. T., W. F. Ruddiman, Q. Z. Hao, H. B. Wu, Y. S. Qiao, R. X. Zhu, S. Z. Peng, J. J. Wei, B. Y. Yuan, and T. S. Liu (2002), Onset of Asian desertification by 22 Myr ago inferred from loess deposits in China, *Nature*, *416*, 159–163.

Heller, F., and M. E. Evans (1995), Loess magnetism, *Rev. Geophys.*, *33*, 211–240.

Heller, F., and T. S. Liu (1982), Magnetostratigraphical dating of loess deposits in China, *Nature*, *300*, 431–433.

Heller, F., and T. S. Liu (1986), Paleoclimatic and sedimentary history from magnetic susceptibility of loess in China, *Geophys. Res. Lett.*, *13*, 1169–1172.

Hunt, C. P., S. K. Banerjee, J. Han, P. A. Solheid, E. Oches, W. Sun, and T. Liu (1995), Rock-magnetic proxies of climate change in the loess-paleosol sequences of the western Loess Plateau of China, *Geophys. J. Int.*, *123*, 232–244.

Janitzky, P. (1986), Citrate-bicarbonate-dithionite (CBD) extractable iron and aluminum, in *Field and Laboratory Procedures Used in a Soil Chronosequence Study*, edited by M. J. Singer and P. Janitzky, pp. 38–40, U.S. Govt. Print. Off., Washington, D. C.

Ji, J., W. Balsam, and J. Chen (2001), Mineralogic and climatic interpretations of the Luochuan loess section (China) based on diffuse reflectance spectrophotometry, *Quat. Res.*, *56*, 23–30.

Kalm, V. E., N. W. Rutter, and C. D. Rokosh (1996), Clay minerals and their paleoenvironmental interpretations in the Baoji loess section, southern Loess Plateau, China, *Catena*, *27*, 49–61.

King, J. W., and J. E. T. Channell (1991), Sedimentary magnetism, environmental magnetism, and magnetostratigraphy, *U.S. Natl. Rep. Int. Union Geod. Geophys. 1987–1990*, *Rev. Geophys.*, *29*, 358–370.

Kukla, G., F. Heller, X. M. Liu, T. C. Xu, T. S. Liu, and Z. S. An (1988), Pleistocene climates in China dated by magnetic susceptibility, *Geology*, *16*, 811–814.

Liu, Q. S., S. K. Banerjee, M. J. Jackson, F. H. Chen, Y. X. Pan, and R. X. Zhu (2003), An integrated study of the grain-size-dependent magnetic mineralogy of the Chinese loess/paleosol and its environmental significance, *J. Geophys. Res.*, *108*(B9), 2437, doi:10.1029/2002JB002264.

Liu, T. S. (1985), *Loess and the Environment*, 251 pp., China Ocean Press, Beijing.

Liu, T., and Z. Ding (1998), Chinese loess and the paleomonsoon, *Annu. Rev. Earth Planet. Sci.*, *26*, 111–145.

Maher, B. A. (1998), Magnetic properties of modern soils and Quaternary loessic paleosols: Paleoclimatic implications, *Palaeogeogr. Palaeoclimatol. Palaeoecol.*, *137*, 25–54.

Maher, B. A., and R. Thompson (1991), Mineral magnetic record of the Chinese loess and paleosols, *Geology*, *19*, 3–6.

Oches, E. A., and S. K. Banerjee (1996), Rock-magnetic proxies of climate change from loess-paleosol sediments of the Czech Republic, *Stud. Geophys. Geodaet.*, *40*, 287–300.

Pan, Y. X., R. X. Zhu, Q. S. Liu, B. Guo, L. P. Yue, and H. N. Wu (2002), Geomagnetic episodes of the last 1.2 Myr recorded in Chinese loess, *Geophys. Res. Lett.*, *29*(9), 1282, doi:10.1029/2001GL014024.

Righi, D., B. Velde, and A. Meunier (1995), Clay stability in clay-dominated soil systems, *Clay Miner.*, *30*, 45–54.

Roberts, A. P., Y. Cui, and K. L. Verosub (1995), Wasp-waisted hysteresis loops: Mineral magnetic characteristics and discrimination of components in mixed magnetic systems, *J. Geophys. Res.*, *100*, 17,909–17,924.

Singer, M. J., P. Fine, K. L. Verosub, and O. A. Chadwick (1992), Time dependence of magnetic susceptibility of soil chronosequences on the California coast, *Quat. Res.*, *37*, 323–332.

Sun, J., and T. Liu (2000), Stratigraphic evidence for the uplift of the Tibetan Plateau between ~1.1 and ~0.9 Myr ago, *Quat. Res.*, *54*, 309–320.

Vandenberghe, R. E., J. J. Hus, and E. De Grave (1998), Evidence from Mössbauer spectroscopy of neo-formation of magnetite/maghemite in the

soils of loess/paleosol sequences in China, *Hyperfine Interact.*, *117*, 359–369.

van Velzen, A. J., and M. J. Dekkers (1999), Low-temperature oxidation of magnetite in loess-paleosol sequences: A correction of rock magnetic parameters, *Stud. Geophys. Geodaet.*, *43*, 357–375.

Verosub, K. L., and A. P. Roberts (1995), Environmental magnetism: Past, present, and future, *J. Geophys. Res.*, *100*, 2175–2192.

Verosub, K. L., P. Fine, M. J. Singer, and J. TenPas (1993), Pedogenesis and paleoclimate: Interpretation of the magnetic susceptibility record of Chinese loess-paleosol sequences, *Geology*, *21*, 1011–1014.

Vidic, N. J., J. D. TenPas, K. L. Verosub, and M. J. Singer (2000), Separation of pedogenic and lithogenic components of magnetic susceptibility in the Chinese loess/paleosol sequence as determined by the CBD procedure and a mixing analysis, *Geophys. J. Int.*, *142*, 551–562.

Xu, L. Z., and X. Z. Wang (2003), *Shaanxi Atlas* (in Chinese), 268 pp., Xi'an Map Press, Xi'an, China.

Zhou, L. P., F. Oldfield, A. G. Wintle, S. G. Robinson, and J. T. Wang (1990), Partly pedogenic origin of magnetic variations in Chinese loess, *Nature*, *346*, 737–739.

Zhu, R., C. Deng, and M. J. Jackson (2001), A magnetic investigation along a NW-SE transect of the Chinese Loess Plateau and its implications, *Phys. Chem. Earth, Part A*, *26*, 867–872.

Zhu, R. X., C. Laj, and A. Mazaud (1994), The Matuyama-Brunhes and Upper Jaramillo transitions recorded in a loess section at Weinan, north-central China, *Earth Planet. Sci. Lett.*, *125*, 143–158.

Zhu, R. X., G. Matasova, A. Kazansky, V. Zykina, and J. M. Sun (2003), Rock magnetic record of the last glacial-interglacial cycle from the Kurtak loess section, southern Siberia, *Geophys. J. Int.*, *152*, 335–343.

C. Deng and R. Zhu, Paleomagnetism Laboratory, Institute of Geology and Geophysics, Chinese Academy of Sciences, Beijing 100029, China. (cldeng@mail.igcas.ac.cn)

M. J. Singer and N. J. Vidic, Department of Land, Air and Water Resources, University of California, 1 Shields Avenue, Davis, CA 95616, USA. (mjsinger@ucdavis.edu; njvidic@ucdavis.edu)

K. L. Verosub, Department of Geology, University of California, Davis, CA 95616, USA. (verosub@geology.ucdavis.edu)